Biophysical Journal
Article

Biophysical Society

Small-Volume Effect Enables Robust, Sensitive, and Efficient Information Transfer in the Spine

Masashi Fujii,[1,2] Kaoru Ohashi,[1] Yasuaki Karasawa,[3] Minori Hikichi,[1] and Shinya Kuroda[1,2,4,*]
[1]Department of Biological Sciences and [2]Molecular Genetics Research Laboratory, Graduate School of Sciences, University of Tokyo, Bukyo-ku, Tokyo, Japan; [3]Department of Neurosurgery, Graduate School of Medicine, University of Tokyo, Bukyo-ku, Tokyo, Japan; and [4]CREST, Japan Science and Technology Agency, Bunkyo-ku, Tokyo, Japan

ABSTRACT Why is the spine of a neuron so small that it can contain only small numbers of molecules and reactions inevitably become stochastic? We previously showed that, despite such noisy conditions, the spine exhibits robust, sensitive, and efficient features of information transfer using the probability of Ca^{2+} increase; however, the mechanisms are unknown. In this study, we show that the small volume effect enables robust, sensitive, and efficient information transfer in the spine volume, but not in the cell volume. In the spine volume, the intrinsic noise in reactions becomes larger than the extrinsic noise of input, resulting in robust information transfer despite input fluctuation. In the spine volume, stochasticity makes the Ca^{2+} increase occur with a lower intensity of input, causing higher sensitivity to lower intensity of input. The volume-dependency of information transfer increases its efficiency in the spine volume. Thus, we propose that the small-volume effect is the functional reason why the spine has to be so small.

INTRODUCTION

The spine is an extremely small structure, where afferent inputs from other neurons are temporally added (1,2). For example, the volume of a spine at the parallel fiber (PF)-cerebellar Purkinje cell synapse is approximately 10^{-1}–1 μm^3 (3). Such volume is 10^4-fold smaller than the cell body (5000 μm^3) and contains merely tens or hundreds of molecules (Fig. 1 *A*; see also Fig. 7) (4–6). Under such conditions, reactions in the spine inevitably become stochastic and inputs fluctuate because of the low number of molecules confined in a small volume (7–11). Intuitively, such noisy conditions are disadvantageous for information processing. Why is the spine so small? This is one of the fundamental questions in neuroscience and biological information processing.

Cerebellar Purkinje cells receive two inputs. One is from more than 100,000 PFs, which are the axons of granular neurons, coding sensorimotor signals. The other input is a single climbing fiber (CF) from the inferior olivary nucleus, which is thought to code an error signal (12–14). A conjunctive activation of PF and CF inputs, but not either the PF input or CF input alone, has been shown to induce large Ca^{2+} increases by the Ca^{2+} inflow through voltage-gated channels and inositol trisphosphate (IP_3)-induced Ca^{2+} release (IICR) (15,16), leading to long-term decreases of synaptic strength that are known as cerebellar long-term depression (LTD) (17), which is a tentative molecular basis of cerebellar motor learning (18,19). It has been experimentally shown that a large Ca^{2+} increase occurs when PF and CF inputs are coincident within a 200-ms time window (Fig. 1 *B*), and that the Ca^{2+} increase as a function of the timing between PF and CF inputs shows a bell-shaped response (Fig. 1 *C*) (16). We have previously developed a detailed biochemical deterministic model of the Ca^{2+} increase in a PF-cerebellar Purkinje cell synapse, reproducing the PF- and CF-timing-dependent Ca^{2+} increases (20). In addition, by reducing this model, we also constructed a simple deterministic model, from which we derived an essential framework of the network for PF- and CF-timing-dependent Ca^{2+} increases (21,22).

However, in the spine, the number of molecules is limited to tens to hundreds; therefore, reactions should behave stochastically rather than deterministically. It has been experimentally shown that the Ca^{2+} increase due to the coincidence of PF and CF inputs behaves stochastically; in some cases, large Ca^{2+} increases are observed, but in other cases they are not large (Fig. 1, *B* and *C*). In addition to the intrinsic noise due to the stochastic fluctuation of the transient increases of the Ca^{2+} concentration, the PF input has been

Submitted November 9, 2016, and accepted for publication December 29, 2016.

*Correspondence: skuroda@bs.s.u-tokyo.ac.jp

Editor: Anatoly Kolomeisky
http://dx.doi.org/10.1016/j.bpj.2016.12.043

© 2017 Biophysical Society.

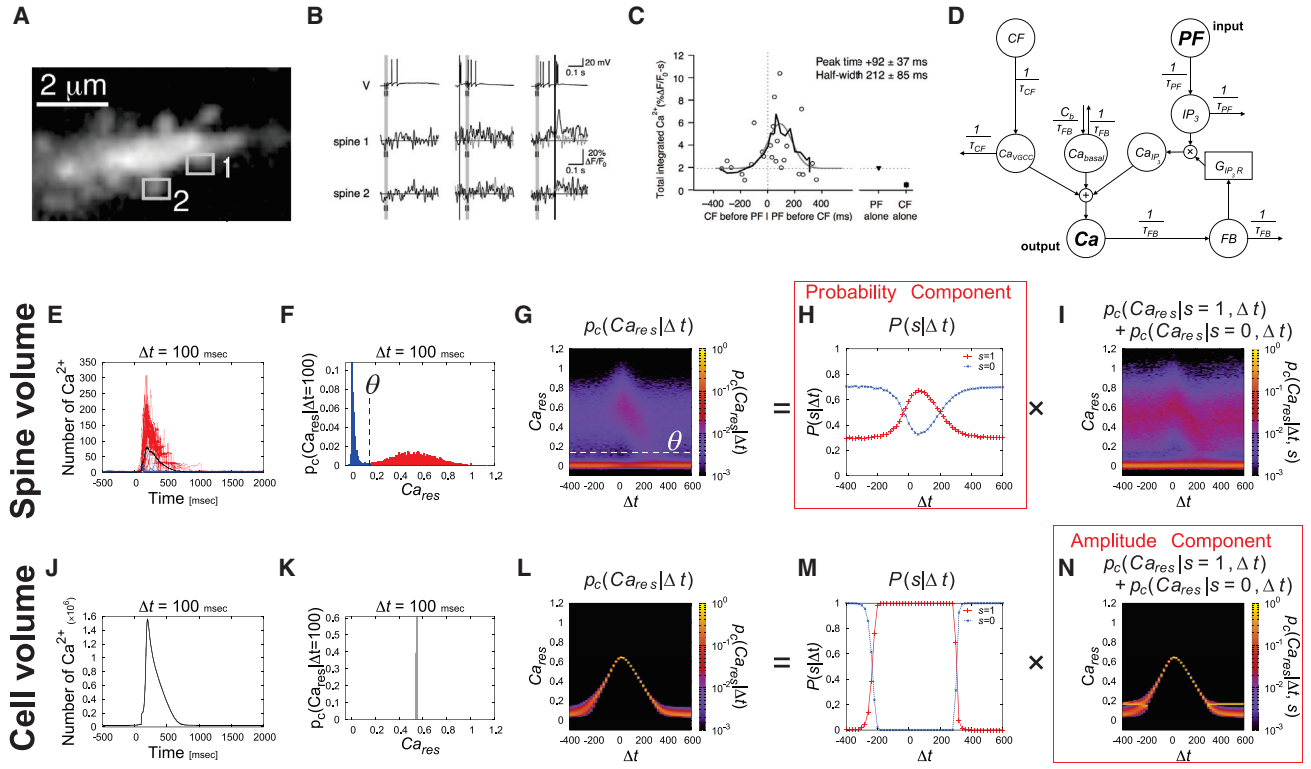

FIGURE 1 Information transfer of PF- and CF-timing by probability of Ca^{2+} increase in the simple stochastic model. (*A–C*) Experimental results of Ca^{2+} increase by PF and CF inputs at the spine in the cerebellar Purkinje cell (16). (*A*) Spines of the cerebellar Purkinje cell are shown. (*B*) Ca^{2+} responses in the indicated spines in (*A*) are shown. V indicates membrane potential and $\Delta F/F_0$ indicates the normalized changes of the fluorescence probe of Ca^{2+}. The left, middle, and right panels show the time courses with only the PF input (*shaded vertical line*), with the CF input (*black vertical line*) 60 ms before the PF input and with the PF input 60 ms before the CF input, respectively. (*C*) Total integrated Ca^{2+} with PF and CF inputs with various timing are shown. The gray line indicates the best fits of the raw data points to Gaussian functions. The black line indicates the box-smoothed average over three points. (*D*) The block diagram of the simple stochastic model in this study (see Materials and Methods) is provided. After Fig. 3, we set $CF = 0$ and used only PF as the input. Ca^{2+} increase in the spine volume (10^{-1} μm^3) (*E–I*) and in the cell volume (10^3 μm^3) (*J–N*) in the simple stochastic model. (*E* and *J*) Ca^{2+} increase with $\Delta t =$ 100 ms is provided. Δt indicates the timing interval between PF and CF inputs, which is the timing of the PF input set as 0 and Δt with the PF input before CF input is positive, and vice versa. (*E*) The large Ca^{2+} increase (*red*) and small Ca^{2+} increase (*blue*) divided by θ in (*F*) are provided. (*F* and *K*) The probability density distribution of Ca_{res} is provided. Ca_{res} denotes the area under the curve of the time course of Ca^{2+}, subtracted by the basal Ca^{2+} concentration, shown in (*E*) and (*J*). (*F*) The threshold θ is defined as the local minimum of the marginal distribution for Δt, given by $p_c(Ca_{res}) = \int_{\Delta t} p_c(Ca_{res} \mid \tau) p_{in}(\tau) d\tau$ (see Fig. S1). (*G* and *L*) The probability density distribution of Ca_{res} in the spine volume (*G*) and cell volume (*L*) are provided. (*H* and *M*) The probability component of the distribution of Ca_{res} that exceeds the threshold θ in the spine volume ($s = 1$) (see Materials and Methods) is provided. Because the distribution of Ca_{res} in the cell volume is unimodal distribution, for convenience, we set $\theta = 0.157$ in the cell volume, which is the same as that in the spine volume. (*I* and *N*) The amplitude component of the distribution of Ca_{res} (see Materials and Methods) is provided. Images are used with permission from Wang et al. (16). To see this figure in color, go online.

shown to fluctuate due to the stochasticity of the glutamate release from the presynapse (9–11), which can be regarded as extrinsic noise. In this study, the extrinsic noise means the PF input fluctuation rather than the different initial conditions such as the molecular concentration/numbers in the individual spines. Based on the deterministic model (20), we constructed a stochastic simulation model of the Ca^{2+} increase depending on PF- and CF-timing incorporating the stochastic reactions due to the small number of molecules (23). We have previously shown that the spine uses the probability of the Ca^{2+} increase, rather than its amplitude, for information transfer, and that the probability of the Ca^{2+} increase in the spine shows robustness against input fluctuation, sensitivity to lower input numbers, and efficiency in information transfer (23). The more detailed definitions of the robustness, sensitivity, and efficiency were described below in the corresponding parts (see Results). However, the robustness, sensitivity, and efficiency were not characterized, and their informatical mechanisms remain unknown.

In this study, we constructed a simple stochastic model based on the simple deterministic model (21). Note that the detailed stochastic model contains a large number of molecules and reactions so that it is hard to perform the stochastic simulation of the deterministic model with various parameters, such as the amplitude of PF inputs. Using the simple stochastic model, we define the robustness, sensitivity, and efficiency of information transfer mediated by the Ca^{2+} increase, and clarify their mechanisms (see

Fig. 7). We defined the robustness as the unchanging distribution of the Ca^{2+} increase against the fluctuation of the PF input, which can be seen under the condition where extrinsic noise caused by the fluctuation of the PF input is much smaller than intrinsic noise caused by stochasticity in the Ca^{2+} increase. The robustness appears against much larger fluctuation of the PF input in the spine volume. We defined the sensitivity as the amplitude of the PF input giving the maximum of information transfer. In the spine volume, stochasticity makes the Ca^{2+} increase occur with a lower intensity of input, causing higher sensitivity to lower intensity of input. We defined the efficiency as how much information can be transferred by a unitary PF input. The volume-dependency of information transfer increases its efficiency in the spine volume. We found that the small-volume effect enables robust, sensitive, and efficient information transfer in the spine volume, but not in the cell volume. We propose that the small-volume effect is one of the functional reasons why the spine has to be so small.

MATERIALS AND METHODS

Simple stochastic model

The block diagram of the simple stochastic model is the same as that of the simple deterministic model (Fig. 1 *E*) (21). The inputs are *PF* and *CF*. After Fig. 3, we set $CF = 0$, and used only *PF* as the input. The output is *Ca*, which is the same as the output of the detailed stochastic model and remains the value of the number of the Ca^{2+} ion.

The total cytosolic Ca^{2+} in the spine of the Purkinje cell, *Ca*, is derived from the three pathways as follows:

$$Ca = Ca_{basal} + Ca_{VGCC} + Ca_{IP_3}, \tag{1}$$

where Ca_{basal}, Ca_{VGCC}, and Ca_{IP_3} denote the basal cytosolic Ca^{2+}, the Ca^{2+} through the voltage-gated Ca^{2+} channel (VGCC) triggered by *CF*, and the Ca^{2+} through the IP_3 receptors of the internal Ca^{2+} store triggered by *PF*, respectively. Ca_{basal} is constantly produced and described by the following:

$$\phi \overset{C_b/\tau_{FB}}{\rightarrow} Ca_{basal} \overset{1/\tau_{FB}}{\rightarrow} \phi, \tag{2}$$

where C_b/τ_{FB} and $1/\tau_{FB}$ denote the production and decay rate constants of Ca_{basal}, respectively. Hereafter, ϕ denotes a fixed value.

Ca_{VGCC} is triggered by *CF* and is described by the following:

$$CF \overset{1/\tau_{CF}}{\rightarrow} Ca_{VGCC} \overset{1/\tau_{CF}}{\rightarrow} \phi, \tag{3}$$

where $1/\tau_{CF}$ denotes the production and decay rate constants of Ca_{VGCC}, respectively. *CF* is given by $Amp_{PF} \times V$ at $t = t_{CF}$, with the volume of the system, *V*.

Ca_{IP_3} is produced as follows. Briefly, *PF* produces IP_3. *Ca* has positive feedback (*FB*) through the activation of the IP_3 receptor (G_{IP_3R}). IP_3 and G_{IP_3R} synergistically induce *Ca* release through IP_3R (Ca_{IP_3}) and IP_3 is triggered by *PF* as follows:

$$PF \overset{1/\tau_{PF}}{\rightarrow} IP_3 \overset{1/\tau_{PF}}{\rightarrow} \phi, \tag{4}$$

where $1/\tau_{CF}$ denotes the production and decay rate constants of IP_3. *PF* is given by $Amp_{PF} \times V$ at $t = t_{CF}$.

The time-delay variable *FB* is described by the following:

$$Ca \overset{1/\tau_{FB}}{\rightarrow} FB \overset{1/\tau_{FB}}{\rightarrow} \phi, \tag{5}$$

where $1/\tau_{FB}$ denotes the production and decay rate constants of *FB*. This decay rate constant also determines the degradation rate of Ca_{IP_3}.

The IP_3 receptor coupled with Ca^{2+}, G_{IP_3R}, is mediated by the positive and negative feedback from *FB* and is given by the nonlinear function, described by the following:

$$G_{IP_3R} = Amp_{G_{IP_3R}} \left\{ \frac{k \times FB}{(k + FB)(K + FB)} \right\}^{n_{G_{IP_3R}}}, \tag{6}$$

where $Amp_{G_{IP_3R}}$, k, K, and $n_{G_{IP_3R}}$ denote the amplitude of feedback, thresholds of *FB* for the positive and negative feedback, and nonlinearity of feedback, respectively.

The *Ca* released from IP_3R, Ca_{IP_3}, is described by the following:

$$Ca_{IP_3} = IP_3 \times \frac{G_{IP_3R}}{V}. \tag{7}$$

These reactions are simulated by the use of Gillespie's method and the τ-leap method (24). For example, in the reaction described by Eq. 3, the number of the Ca^{2+} from VGCC, $Ca_{VGCC}(t + \tau)$, is described as follows:

$$Ca_{VGCC}(t + \tau) = Ca_{VGCC}(t) + R_{in} - R_{out}, \tag{8}$$

where R_{in} and R_{out} indicate the number of reactions of inflow and outflow, which occur in the time interval between t and $t + \tau$, generated to obey the Poisson distribution, $R_{in} \sim Poisson\ (CF \times \tau/\tau_{CF})$ and $R_{out} \sim Poisson\ (Ca_{VGCC} \times \tau/\tau_{CF})$, respectively. Similarly, the probability of reactions is based on the law of mass action. The appropriate τ is calculated in accordance with by Gillespie et al. (25), which shows good approximation for first-order reactions.

Note that, under normal circumstances, the reactions by membrane molecules on the membrane, such as receptors, and those by cytosolic molecules, such as Ca^{2+} and IP_3, should be considered as separate mechanisms and compartments, which may be affected by the ratio between surface area and volume. In general, the surface area of the membrane is proportional to the order of the square of length, whereas the cell volume is proportional to the cube of that, which means that, as a system size increases, the increasing rate of the number of membrane molecules becomes smaller than that in the cytoplasm. Hence, in the cases of larger systems than the spine, the number of membrane molecules that can activate the cytosolic molecules is so small that most of substrates are not activated by the stimulation. Actually, when a volume was 8- or 125-fold larger than a spine volume, large Ca^{2+} increases did not occur any more at any PF-CF intervals. To uncover the simple influences of the smallness of a spine and the number of molecules, it is required that the effect of the stimulation to the cytosolic molecules through the membrane protein for a cell is the same as that for the spine. Therefore, we assumed that the number of membrane proteins is proportional to the volume, i.e., the cube of length, throughout this study.

We defined Ca_{res} as the area under the curve of the time course of Ca^{2+}, given by the following:

$$Ca_{res} = \int_T \{[Ca](t) - C_b\} dt, \tag{9}$$

where C_b denotes the basal concentration of Ca^{2+}, which is 41.6 nM. Note that Koumura et al. (23) defined Ca_{res} as the logarithmic area under the curve, which is different from that in this study; however, the results of this study qualitatively show the same results.

The values of the parameters in the simple stochastic model are shown in Tables S1 and S2. The parameters excluding the following are the same as those of the simple deterministic model (23).

Mutual information between PF- and CF-timing and Ca^{2+} increase

We measured the input timing information coded by the Ca^{2+} response to mutual information between the Ca_{res} and the PF–CF timing interval $\Delta t = t_{CF} - t_{PF}$, given by the following:

$$I(Ca_{res};\Delta t) = \int_{\Delta t} p_{in}(\tau) \times \left(\int_{Ca_{res}} p_c(c\,|\,\tau)\log_2 \frac{p_c(c\,|\,\tau)}{\int_{\Delta t} p_{in}(\tau)p_c(c\,|\,\tau)d\tau}\,dc \right) d\tau. \tag{10}$$

Here, the p_{in} (Δt) follows the uniform distribution. To remove the bias caused by the bin width of Ca_{res}, the mutual information was calculated by the method introduced by Cheong et al. (26). The mutual information remains almost constant for the bin width between 10^{-2} and $10^{-3.5}$ (pM min). Therefore, we fixed the bin width of Ca_{res} as 10^{-2} (pM min) in the analysis and for drawing the histogram.

We also measured the information coded by the probability of the large Ca^{2+} increase and by the amplitude of the Ca^{2+} increase, denoted as the mutual information of the probability component and of the amplitude component, respectively. We defined θ as the Ca_{res} representing the local minimum value of the marginal distribution p_c (Ca_{res}) (Fig. 1 *F*) and s as the logical value, whether $Ca_{res} > \theta$ is satisfied or not.

The mutual information coded with the probability component, which indicates the information transfer coded by the probability whether the large Ca^{2+} increase occurs or not, is defined as follows:

$$I_{prob}(Ca_{res};\Delta t) = \int_{\Delta t} p_{in}(\tau) \times \left(\int_{Ca_{res}} p_c(c\,|\,\tau)\log_2 \frac{p_c(c\,|\,\tau)}{p_{-prob}(c\,|\,\tau)}\,dc \right) d\tau, \tag{11}$$

and

$$p_{-prob}(Ca_{res}\,|\,\Delta t) = \sum_{s\in\{0,1\}} P(s)p_c(Ca_{res}\,|\,s,\Delta t), \tag{12}$$

where p_{-prob} $(Ca_{res}|\Delta t)$ denotes the distribution of Ca_{res} without the probability component, which was calculated by marginalizing Δt out of the probability component P $(s|\Delta t)$ in p_c $(Ca_{res}|\Delta t)$.

The mutual information coded by the amplitude component, which indicates the information transfer coded by the amplitude of the Ca^{2+} increase, is defined as follows:

$$I_{amp}(Ca_{res};\Delta t) = \int_{\Delta t} p_{in}(\tau) \times \left(\int_{Ca_{res}} p_c(c\,|\,\tau)\log_2 \frac{p_c(c\,|\,\tau)}{p_{-amp}(c\,|\,\tau)}\,dc \right) d\tau, \tag{13}$$

and

$$p_{-amp}(Ca_{res}\,|\,\Delta t) = \sum_{s\in\{0,1\}} P(s\,|\,\Delta t)p_c(Ca_{res}\,|\,s), \tag{14}$$

where p_{-amp} $(Ca_{res}|\Delta t)$ denotes the distribution of Ca_{res} without the amplitude component, which was calculated by marginalizing Δt out of the amplitude component P $(s|\Delta t)$ in $p_c(Ca_{res}\,|\,\Delta t)$. This information satisfies the following:

$$I(Ca_{res};\Delta t) = I_{prob}(Ca_{res};\Delta t) + I_{amp}(Ca_{res};\Delta t). \tag{15}$$

Note that I_{prob} mathematically indicates the information transfer coded by the probability of the large Ca^{2+} increase, i.e., the probability component, whereas I_{amp} actually indicates the information transfer coded by other than the probability of the large Ca^{2+} increase, including the amplitude of the Ca^{2+} increase, i.e., the amplitude component. However, the amplitude component seems to be dominant component in that expect for the probability component. Thus, we defined I_{prob} and I_{amp} as the information coded with probability and amplitude components, respectively.

Mutual information between the amplitude of PF input and Ca^{2+} increase

We also calculated the mutual information between Ca_{res} and Amp_{PF} by assuming the input distribution as the Gaussian distribution with μ_s, the average, and STD, the SD, given by the following:

$$I(Ca_{res};Amp_{PF}) = \int_{Amp_{PF}} p_s(a\,|\,\mu_s,STD)\left(\int_{Ca_{res}} p_c(c\,|\,a)\log_2 \frac{p_c(c\,|\,a)}{\int_{Amp_{PF}} p_s(a\,|\,\mu_s,STD)p_c(c\,|\,a)da}\,dc \right) da \tag{16}$$

where

$$p_s(Amp_{PF}|\mu_s,STD) = \frac{1}{\sqrt{2\pi STD^2}}\exp\left[-\frac{(Amp_{PF}-\mu_s)^2}{2STD^2} \right]. \tag{17}$$

Note that below in Results, we defined p_a as the probability density distribution of the PF input fluctuation and is assumed as a Gaussian distribution.

Therefore, p_s and p_a have Amp_{PF} as the variable and are assumed as a Gaussian distribution. However, these distributions mean different features: p_s means the input distribution of the mutual information, and p_a means the distribution of amplitude of the PF input under the fluctuation of amplitude of the PF input.

Fitted function of the volume-dependency of mutual information

The mutual information per the PF input against the volume was fitted by the functions $a \log_2 (b + c \times V)$ and $1/2 \log_2 (1 + c \times V)/V$ (see Fig. 6 *B*) by using of the nonlinear least squares method with the Marquadt-Levenberg algorithm. We obtained the fitting line, $a \log_2 (b + c \times V)$, with the best fit of $a = 0.3924651$, $b = 1.049141$, and $c = 1.330285$ and the channel capacity of the Gaussian channel, $1/2 \log_2 (1 + c \times V)$, with the best fit parameter of $c = 0.5128671$.

RESULTS

Development of the simple stochastic model

To reduce the complexity and computational cost of the detailed stochastic model (23), we constructed the simple stochastic model based on the simple deterministic model (Fig. 1 *D*) (21). We set the parameters according to the PF and CF inputs of the simple deterministic model to reproduce the PF- and CF-timing dependent Ca^{2+} responses of the detailed stochastic model (23) (Fig. 1; see Materials and Methods; Tables S1 and S2). Thereafter, we denoted 10^{-1} μm^3 as the spine volume, and 10^3 μm^3 as the cell volume. In the spine volume, coincident PF and CF inputs with $\Delta t = 100$ ms induced a large Ca^{2+} increase (Fig. 1 *E*, *red*), but they sometimes failed to induce a large Ca^{2+} increase (Fig. 1 *E*, *blue*). We defined Ca_{res} as the temporal integration of the Ca^{2+} concentration, subtracted by the basal Ca^{2+} concentration. The distribution of Ca_{res} showed a bimodal distribution (Fig. 1 *F*). The distribution of Ca_{res} always showed a bimodal distribution regardless of the timing between the PF and CF inputs, and probability of a large Ca^{2+} increase changed depending on the timing between the PF and CF inputs (Fig. 1 *G*). We divided the distribution of Ca_{res} into the probability component (Fig. 1 *H*) and the amplitude component (Fig. 1 *I*) (see Materials and Methods). The probability component, but not the amplitude component, showed a bell-shaped time window, indicating that the timing information between the PF and CF inputs is coded by the probability of a large Ca^{2+} increase, rather than by the amplitude of the Ca^{2+} increase in the spine volume. In contrast, in the cell volume, the coincident PF and CF inputs with $\Delta t = 100$ ms always induced a large Ca^{2+} increase without failure (Fig. 1 *J*) and Ca_{res} showed a unimodal distribution (Fig. 1 *K*) (see Materials and Methods). The distribution of Ca_{res} always showed a unimodal distribution regardless of the timing between the PF and CF inputs (Fig. 1 *L*), and only the amplitude of Ca_{res} (Fig. 1 *N*), not the probability (Fig. 1 *M*), showed a bell-shaped time window, indicating that the timing information between the PF and CF inputs is coded by the amplitude of the Ca^{2+} increase, rather than the probability of a large Ca^{2+} increase in the cell volume. These results are consistent with our previous study using the detailed stochastic model (23).

The simple stochastic model also showed similar properties, such as efficiency, robustness, and sensitivity in the detailed stochastic model (Fig. 2; see Fig. S2). Mutual information is a nonlinear measure of correlation that takes into account entire probability distributions rather than simply second-order correlations, and a quantitative measure of how much information is transferred from input to output (27). We used mutual information as a measure of how much information is transferred from the PF- and CF-timing to Ca_{res}. The mutual information between the PF- and CF-timing and Ca_{res} increased with the increase in volume (Fig. 2 *A*). In the spine volume, the probability component of the mutual information was larger than the amplitude component of the mutual information (Fig. 2 *A*, *inset*), and the amplitude component of the mutual information became larger than the probability component of the mutual information with increase in the volume. Mutual information per volume became highest at the spine volume, and it decreased with the increase in volume (Fig. 2 *B*), indicating that the most-efficient information coding per volume is achieved at the spine volume. In the spine volume, the mutual information did not decrease; it remained constant regardless of the coefficient of variation (CV) of the PF input (Fig. 2 *C*, *black line*), whereas that in the cell volume decreased with the increase in CV of the PF input (Fig. 2 *C*, *yellow line*; see Fig. S1), indicating that the information

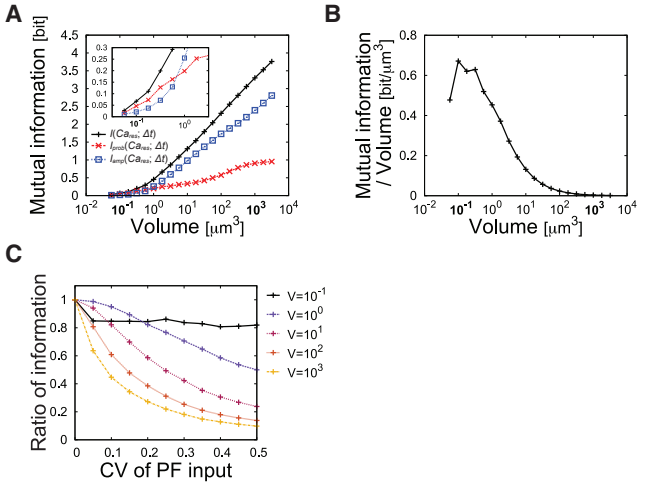

FIGURE 2 The efficient and robust features in the simple stochastic model. (*A*) The volume-dependency of the mutual information between the PF- and CF-timing and Ca_{res} is provided. Black, red, and blue lines indicate the mutual information of the total distribution of Ca_{res}, of the probability component, and of the amplitude component, respectively. (*B*) The volume-dependency of the mutual information per volume. (*C*) CV of amplitude of the PF input-dependency of the mutual information. The ratio of information was obtained by setting mutual information with CV = 0 for each volume at 1. To see this figure in color, go online.

transfer by Ca_{res} is robust against fluctuation of the PF input in the spine volume only, but not in the larger volume including the cell volume. The detailed stochastic model showed higher sensitivity to the lower numbers of the PF input in the spine volume rather than that in the cell volume (see Fig. S2 D) (23). We showed that the higher sensitivity to lower PF input can be seen in the spine volume, but not in the larger volume including the cell volume (see below). These results of the simple stochastic model are also consistent with those of the detailed stochastic model (see Fig. S2) (23).

These results indicate that the simple stochastic model can retain the essential properties of the Ca^{2+} response, such as robust, sensitive, and efficient features. Using this simple stochastic model, we next defined the robustness, sensitivity, and efficiency, and clarified their mechanisms in the spine volume.

The mechanism of robustness

In this section, we define the robustness and clarify the mechanism of the robustness. The amplitudes of the Ca^{2+} increase by conjunctive PF and CF inputs is compatible with those by strong PF input alone (see Fig. S3 *K*) (20). Consistently, strong PF input alone has experimentally been shown to induce a large Ca^{2+} increase (28). Therefore, we hereafter used the PF input alone for simplicity. First, we showed that robustness is provided by the unchanging distribution of Ca_{res} against the fluctuation of the PF input. We obtained the necessary and sufficient condition for robustness, where the intrinsic noise is much larger than the extrinsic noise. We showed that the range of the PF input fluctuation satisfying the conditions for robustness is much larger in the spine volume than in the cell volume, indicating that the distribution of Ca_{res} against the fluctuation of the PF input in the spine volume is more robust than in the cell volume against the fluctuation of the PF input.

Hereafter, we used only the PF input alone instead of PF and CF inputs. Amp_{PF}, the amplitude of the PF input, was set to be between 150 and 215 because the range of amplitude of the PF input alone corresponds to the range of amplitude of the PF- and CF-timing dependent inputs (see Fig. S3 *K*). Therefore, with the appropriate distribution of the PF input as the input distribution of the amplitude of the PF input, the mutual information between the PF- and CF-timing interval and Ca_{res} could be calculated from the Amp_{PF}-dependent distributions of the Ca_{res}. We performed the stochastic simulation 10^4 times per each amplitude of the PF input, which is defined as Amp_{PF}, and obtained p_c $(Ca_{res}|Amp_{PF})$, the probability density distribution of Ca_{res}. Using p_c $(Ca_{res}|Amp_{PF})$, we examined the mechanism of robustness. In the spine volume, the distribution of Ca_{res}, p_c $(Ca_{res}|Amp_{PF})$, became bimodal when Amp_{PF} exceeded ~50 (Fig. 3 *A*; Fig. S3, *A* and *B*). In contrast, in the cell volume, the distribution of Ca_{res} always showed unimodal distribution regardless of Amp_{PF}, and its average monotonically increased along Amp_{PF} when Amp_{PF} exceeded ~150 (Fig. 3 *B*; Fig. S3, *I* and *J*).

The robustness is given by the unchanging distribution of Ca_{res} *against the fluctuation of PF input*

We have shown that the distribution of Ca_{res} for each Δt was unchanged regardless of CV of the PF input in the spine volume, but not in the cell volume (see Fig. S1) (23), suggesting that the unchanging distribution of Ca_{res} against the fluctuation of the PF input is a key to the robustness of the information transfer. Therefore, we examined whether the distribution of Ca_{res} with the PF input alone is also unchanged regardless of CV of the PF input in the spine volume, but not in the cell volume.

Experimentally, it has been reported that the distribution of the amplitude of the PF input in the Purkinje cell can be approximated by a Gaussian distribution (11). We set p_a $(Amp_{PF} \mid \mu_a, \sigma_a)$, the probability density distribution of Amp_{PF}, as the Gaussian distribution given by $\mathcal{N}(Amp_{PF} \mid \mu_a, \sigma_a^2)$, where μ_a and σ_a denote the average of Amp_{PF} and the SD of Amp_{PF} b, respectively. We used σ_a, the SD of Amp_{PF}, as the magnitude of fluctuation of Amp_{PF} because the σ_a is proportional to CV_a, the CV of Amp_{PF}, with the fixed μ_a, given by $CV_a = \sigma_a/\mu_a$. When the PF input is given by p_a $(Amp_{PF} \mid \mu_a, \sigma_a)$, p_{ac} $(Ca_{res} \mid \mu_a, \sigma_a)$, the distribution of Ca_{res} with the fluctuation of Amp_{PF}, is given by the following:

$$\begin{aligned} p_{ac}(Ca_{res} \mid \mu_a, \sigma_a) &= \int_{Amp_{PF}} p_a(a \mid \mu_a, \sigma_a) p_c(Ca_{res} \mid a) da \\ &= \int_{Amp_{PF}} \mathcal{N}\left(a \mid \mu_a, \sigma_a^2\right) p_c(Ca_{res} \mid a) da, \end{aligned} \tag{18}$$

where p_c $(Ca_{res}|a)$ for each $a \in Amp_{PF}$, i.e., p_c $(Ca_{res}|Amp_{PF})$, was obtained by the stochastic simulation. In the spine volume, the distributions of Ca_{res} always exhibited similar bimodal distributions regardless of CV_a and did not change even if the CV_a became larger (Fig. 3, *C–E*). In contrast, in the cell volume, the distributions of Ca_{res} exhibited unimodal distribution with $CV_a = 0$; with the increase in CV_a, the distributions of Ca_{res} changed and became bimodal (Fig. 3, *F–H*). These properties remained the same regardless of μ_a, the average of Amp_{PF} (see Fig. S4). Similar results were obtained when both PF and CF inputs were used (see Fig. S1).

Taken together, in the spine volume, the distribution of Ca_{res} remained almost unchanged against the fluctuation of Amp_{PF}, whereas, in the cell volume, the distribution of Ca_{res} largely varied against the fluctuation of Amp_{PF}. These results indicate that the unchanging distribution of Ca_{res} against the fluctuation of Amp_{PF} causes robustness. Note

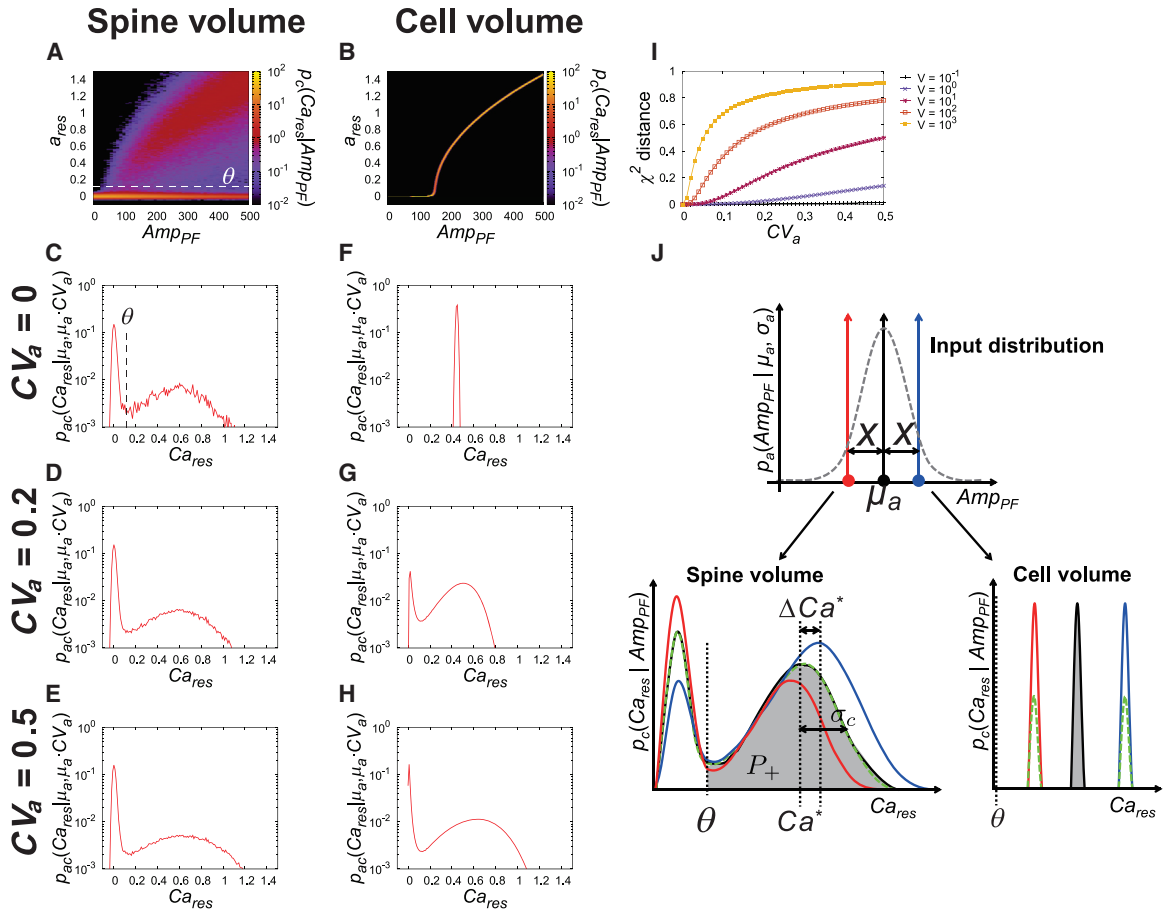

FIGURE 3 Unchanging distributions of Ca_{res} against fluctuation of the PF input gives robustness in the spine volume. The Amp_{PF}-dependency of p_c ($Ca_{res}|Amp_{PF}$) and the distributions of Ca_{res} in the spine volume (*A*) and in the cell volume (*B*) are shown. (*C–H*) The distributions of Ca_{res} against the PF input fluctuation with the indicated CV_a with $\mu_a = 180$ in the spine volume (*C–E*) and in the cell volume (*F–H*), respectively, are shown. θ indicates the threshold dividing the distribution into the ranges with large Ca_{res} and with small Ca_{res} (see Fig. S1). (*I*) The CV_a-dependency of χ^2 distance of distributions between p_{ac} ($Ca_{res} \mid \mu_a, \mu_a \times CV_a$) and p_{ac} ($Ca_{res} \mid \mu_a, 0$) with $\mu_a = 180$. (*J*) The input distribution of Amp_{PF} is given by the Gaussian distribution $\mathcal{N}$ (μ_a, $\sigma_a{}^2$). The distribution of Ca_{res} with $Amp_{PF} = \mu_a$ (*black*), $Amp_{PF} = \mu_a + x$ (*blue*), and $Amp_{PF} = \mu_a - x$ (*red*) in the spine volume (*left*) and in the cell volume (*right*). The averaged distribution with $Amp_{PF} = \mu_a + x$ and with $Amp_{PF} = \mu_a - x$ (*green*). To see this figure in color, go online.

that, in general, the robustness appears not only when the distribution of output does not change by the fluctuation, but also when the distribution drastically changes if the same mutual information can be represented by completely different distributions. However, in the biological systems, it is reasonable to assume that the distribution of the output continuously changes and varies with the increase in the fluctuation of input. Therefore, we did not considered the latter case but considered the robustness only with the unchanging distribution of Ca_{res} against the fluctuation of Amp_{PF}.

We quantitated the change of the distributions of Ca_{res} with the increase in CV_a by the χ^2 distance against the distributions of Ca_{res} with $CV_a = 0$. Note that, in general, the distance between two distributions is calculated by other distance functions, such as KL-divergence, Hellinger distance, etc. However, the χ^2 distance can also reproduce the distance between two distributions, does not diverge, and clearly shows whether the distributions are the same or not. The χ^2 distance becomes 0 when the distribution of Ca_{res} with CV_a is the same as that with $CV_a = 0$, and the χ^2 distance becomes 1 when two distributions are completely different. In the spine volume, the χ^2 distance remained almost 0 regardless of CV_a, whereas in the cell volume the χ^2 distance abruptly increased with the increase in CV_a and became close to 1 (Fig. 3 *I*), indicating that the distribution of Ca_{res} in the spine volume does not change with the increase in CV_a but that in the cell volume largely changes even with a small increase in CV_a. This is the reason why the robustness can be seen only in the spine volume but not in the cell volume.

The necessary and sufficient condition for the robustness

Next, we clarified how the distribution of Ca_{res} in the spine volume does not change with the increase in CV_a, and how that in the cell volume largely changes even with a small

increase in CV_a. We obtained the necessary and sufficient conditions for robustness: unchanging distribution of Ca_{res} regardless of CV_a. We considered p_{ac} ($Ca_{res} \mid \mu_a, \sigma_a$), the distribution of Ca_{res} with the fluctuation of Amp_{PF}, with the increase in CV_a. Note that $CV_a = \sigma_a/\mu_a$). Because $\mathcal{N}(Amp_{PF} \mid \mu_a, \sigma_a^2)$ is symmetric with respect to μ_a, i.e., $\forall a \in Amp_{PF}$, $\mathcal{N}(a \mid \mu_a, \sigma_a^2) = \mathcal{N}(2\mu_a - a \mid \mu_a, \sigma_a^2)$, Eq. 18 was changed as follows:

$$\begin{aligned} p_{ac(Ca_{res} \mid \mu_a, \sigma_a)} &= \int_{\mu_a}^{\infty} \mathcal{N}\left(a \mid \mu_a, \sigma_a^2\right) p_c(Ca_{res} \mid a) da + \int_{-\infty}^{\mu_a} \mathcal{N}\left(a \mid \mu_a, \sigma_a^2\right) p_c(Ca_{res} \mid a) da \\ &= \int_{\mu_a}^{\infty} \mathcal{N}\left(a \mid \mu_a, \sigma_a^2\right) p_c(Ca_{res} \mid a) da + \int_{\mu_a}^{\infty} \mathcal{N}\left(2\mu_a - a \mid \mu_a, \sigma_a^2\right) p_c(Ca_{res} \mid 2\mu_a - a) da \\ &= \int_{\mu_a}^{\infty} \left[\mathcal{N}\left(a \mid \mu_a, \sigma_a^2\right) p_c(Ca_{res} \mid a) + \mathcal{N}\left(a \mid \mu_a, \sigma_a^2\right) p_c(Ca_{res} \mid 2\mu_a - a)\right] da \\ &= \int_{\mu_a}^{\infty} \mathcal{N}\left(a \mid \mu_a, \sigma_a^2\right) [p_c(Ca_{res} \mid a) + p_c(Ca_{res} \mid 2\mu_a - a)] da. \end{aligned} \tag{19}$$

Because the distribution of Amp_{PF} is the Gaussian distribution, $\mathcal{N}(Amp_{PF} \mid \mu_a, \sigma_a^2)$, the probability density of $Amp_{PF} = a$ decreases as the difference between a and μ_a becomes larger. In particular, the probability that $Amp_{PF} = a$ is included in the range $\mu_a - 3\sigma_a \le a \le \mu_a + 3\sigma_a$ is given by $\int_{\mu_a - 3\sigma_a}^{\mu_a + 3\sigma_a} \mathcal{N}(a \mid \mu_a, \sigma_a^2) da = 0.9974\ldots$, i.e., almost 1. Thus, the probability of $a > \mu_a + 3\sigma_a$ or $a < \mu_a - 3\sigma_a$ is quite small and almost negligible. Therefore, satisfying Eq. 19 in the range $\mu_a - 3\sigma_a \le a \le \mu_a + 3\sigma_a$ is enough to satisfy Eq. 19 for almost all ranges of Amp_{PF}. This means that right side of Eq. 19 in the range $a > \mu_a + 3\sigma_a$ can be neglected, and p_{ac} ($Ca_{res} \mid \mu_a, \sigma_a$) is given by the following:

$$\begin{aligned} p_{ac}(Ca_{res} \mid \mu_a, \sigma_a) = \int_{\mu_a}^{\mu_a + 3\sigma_a} & \mathcal{N}\left(a \mid \mu_a, \sigma_a^2\right) [p_c(Ca_{res} \mid a) \\ & + p_c(Ca_{res} \mid 2\mu_a - a)] da. \end{aligned} \tag{20}$$

Here, we considered the case whereby the averaged distribution between the distributions of Ca_{res} with the $Amp_{PF} = a$ shifted $\mid a - \mu_a \mid$ from μ_a, the average of Amp_{PF}, i.e., $1/2[p_c(Ca_{res} \mid a) + p_c(Ca_{res} \mid 2\mu_a - a)]$, is almost the same as the distribution of Ca_{res} with $Amp_{PF} = \mu_a$, p_c ($Ca_{res} \mid \mu_a$) up to $a = \mu_a + 3\sigma_a$, given by the following:

$$\begin{aligned} \forall a < \mu_a + 3\sigma_a : \; p_c(Ca_{res} \mid \mu_a) \simeq & \frac{1}{2} [p_c(Ca_{res} \mid a) \\ & + p_c(Ca_{res} \mid 2\mu_a - a)]. \end{aligned} \tag{21}$$

When the conditions where Eq. 21 is satisfied, we obtained the condition where $p_{ac}(Ca_{res} \mid \mu_a, \sigma_a)$, the distribution of Ca_{res} with the fluctuation of Amp_{PF}, does not change regarding σ_a, the magnitude of fluctuation of Amp_{PF}. This condition means that the distribution of Ca_{res} remained the same with fluctuation of Amp_{PF}. Substituting Eq. 21 for Eq. 20, we obtained the following:

$$\begin{aligned} p_{ac}(Ca_{res} \mid \mu_a, \sigma_a) &\simeq 2 \int_{\mu_a}^{\mu_a + 3\sigma_a} \mathcal{N}\left(a \mid \mu_a, \sigma_a^2\right) p_c(Ca_{res} | \mu_a) da \\ &= 2 p_c(Ca_{res} \mid \mu_a) \int_{\mu_a}^{\mu_a + 3\sigma_a} \mathcal{N}\left(a \mid \mu_a, \sigma_a^2\right) da \\ &\simeq p_c(Ca_{res} \mid \mu_a). \end{aligned} \tag{22}$$

The left side of Eq. 22 indicates the distribution of Ca_{res} with fluctuation of Amp_{PF}. The left side is almost the same with the right side of the equation, which is the distribution of Ca_{res} without fluctuation of Amp_{PF}. Note that σ_a does not directly appear in Eq. 21; however, σ_a determines the upper bound of the range of $a - \mu_a$ satisfying Eq. 21. This means that if Eq. 22 is satisfied for $\sigma_a = \sigma_a^*$, then Eq. 22 is also satisfied for $\sigma_a < \sigma_a^*$. Namely, the upper bound of range $a - \mu_a$ satisfying Eq. 21 is larger, and Eq. 22 is satisfied for larger σ_a, i.e., CV_a. Therefore, Eq. 21 is the condition sufficient to allow the distribution of Ca_{res} not to change against the fluctuation of Amp_{PF}.

Taken together, Eq. 21 is a necessary and sufficient condition in which the distribution of Ca_{res} remains the same against the fluctuation of Amp_{PF}. If $a - \mu_a$, the effective Amp_{PF} with fluctuation of Amp_{PF}, satisfying Eq. 21 is larger, then the distribution of Ca_{res} does not change, even with the larger fluctuation of Amp_{PF}. Therefore, the upper bound of range $a - \mu_a$ satisfying Eq. 21 determines the maximum of σ_a, where the distribution of Ca_{res} does not change. Next, we examined the upper bounds of range $a - \mu_a$ satisfying Eq. 21 in the spine volume and in the cell volume. We also demonstrated that the upper bound of range $a - \mu_a$

satisfying Eq. 21 in the spine volume is much larger than that in the cell volume; therefore, information transfer by Ca_{res} in the spine volume is much more robust than that in the cell volume against fluctuation of Amp_{PF}.

The necessary and sufficient condition for robustness are satisfied in the range in which the intrinsic noise is larger than the extrinsic noise

We next show that the upper bound of the range of Amp_{PF} satisfying Eq. 21 is determined by the upper bound of the range of Amp_{PF}, where the intrinsic noise is larger than the extrinsic noise. We first provide an intuitive interpretation of this proposition using schematic representation of the distribution of Ca_{res} with the indicated Amp_{PF} in the spine volume and cell volume (Fig. 3 *J*; see Fig. S3), which then we prove. The distribution of Ca_{res} in the spine volume is divided into two distributions by threshold θ (Fig. 3 *J*; see Fig. S3). Note that because of the unimodal distribution of Ca_{res} in the cell volume, we set $\theta = -\infty$ in the cell volume. This means that Eq. 21 was divided into the forms given by the following:

$$p_c(Ca_{res}\,|\,Amp_{PF}) = P_+(Amp_{PF})p_c(Ca_{res}\,|\,Ca_{res} > \theta, Amp_{PF}) + P_-(Amp_{PF})p_c(Ca_{ress}\,|\,Ca_{res} \le \theta, Amp_{PF}), \tag{23}$$

and

$$\begin{cases} P_+(Amp_{PF}) \equiv \int_{\theta}^{\infty} p_c(c\,|\,Amp_{PF})dc \\ P_-(Amp_{PF}) \equiv \int_{-\infty}^{\theta} p_c(c\,|\,Amp_{PF})dc \end{cases}, \tag{24}$$

where P_+ and P_- denote the probabilities of $Ca_{res} > \theta$ and $Ca_{res} \le \theta$ with $Amp_{PF} = a$, respectively. We separately considered the first term and second term of the right side. It should be noted that because θ in the cell volume was set at $-\infty$, P_+ in the cell volume is always 1 for any Amp_{PF}. Furthermore, we defined $x = Amp_{PF} - \mu_a$, the relative amplitude of the PF input, as the difference of Amp_{PF} compared with μ_a, the average of Amp_{PF}. Then, Eqs. 21 and 23 were rewritten, respectively, as follows:

$$p_c(Ca_{res}\,|\,\mu_a) = \frac{1}{2}[p_c(Ca_{res}\,|\,\mu_a + x) + p_c(Ca_{res}\,|\,\mu_a - x)] \tag{25}$$

and

$$p_c(Ca_{res}\,|\,\mu_a + x) = P_+(\mu_a + x)p_c(Ca_{res}\,|\,Ca_{res} > \theta, \mu_a + x) + P_-(\mu_a + x)p_c(Ca_{ress}\,|\,Ca_{res} \le \theta, \mu_a + x). \tag{26}$$

In the spine volume, the distributions of Ca_{res} above the threshold θ with $Amp_{PF} = \mu_a + x$ (Fig. 3 *J*, *blue in the left panel*) and with $Amp_{PF} = \mu_a - x$ (Fig. 3 *J*, *left panel*, *red line*) had $\sigma_c(\mu_a \pm x)$, the SD of Ca_{res}, which is larger than ΔCa^*, the gap of the mode of the distribution of Ca_{res}, and these distributions widely overlapped each other. Then, the averaged distribution of these two distributions of Ca_{res} with $Amp_{PF} = \mu_a \pm x$ became the unimodal and intermediate distribution (Fig. 3 *J*, *green dashed line in left panel*), and became almost the same as the distribution of Ca_{res} above threshold θ with $Amp_{PF} = \mu_a$ (Fig. 3 *J*, *black line in the left panel*). Also, the distributions of Ca_{res} below threshold θ exhibited similar unimodal distribution. Thus, the averaged distribution of these two distributions below threshold θ (Fig. 3 *J*, *green dashed line in left panel*) became almost the same as the distribution of Ca_{res} below the threshold θ with $Amp_{PF} = \mu_a$ (Fig. 3 *J*, *black line in left panel*). Therefore, in the spine volume, for the distributions of Ca_{res} above and below the threshold θ, the averaged distributions of the distributions of Ca_{res} with $Amp_{PF} = \mu_a \pm x$ were the same as that with $Amp_{PF} = \mu_a$, indicating that Eq. 21 is satisfied. This also means that any symmetrical distribution of x other than the Gaussian distribution can give the same result. In contrast, in the cell volume, the distributions of Ca_{res} with $Amp_{PF} = \mu_a + x$ (Fig. 3 *J*, *red line in right panel*) and $Amp_{PF} = \mu_a - x$ (Fig. 3 *J*, *blue line in right panel*) had the SDs that are smaller than ΔCa^*, the gap of the mode of the distribution of Ca_{res}, and did not overlap each other. Then, the averaged distribution of these two distributions (Fig. 3 *J*, *green dashed line in right panel*) became bimodal and did not conform to the distribution of Ca_{res} with $Amp_{PF} = \mu_a$ (Fig. 3 *J*, *black line in right panel*), indicating that Eq. 21 is not satisfied. Therefore, the symmetry of the distribution of Amp_{PF} and large σ_c, the SDs of the distribution of Ca_{res}, in comparison with ΔCa^*, the gap of the mode of the distribution of Ca_{res}, can provide conformation to the averaged distribution of the two distributions of Ca_{res} with $Amp_{PF} = \mu_a \pm x$ to the distribution with $Amp_{PF} = \mu_a$. Then, we proved this proposition. For this purpose, we derived the upper bound of the range of x where Eq. 21 is satisfied, and showed that this upper bound in the spine volume is larger than that in the cell volume.

We examined Eq. 21 as satisfied when σ_c, the SD of Ca_{res}, is larger than ΔCa^*; the gap of Ca^*, the mode of the distribution of Ca_{res}; with $Amp_{PF} = \mu_a + x$ and $Amp_{PF} = \mu_a - x$ (see Supporting Material). We approximately showed that, if Ca^* and P_+ linearly increase with the increase in Amp_{PF}, when $\Delta Ca^* \ll \sigma_c$, then Eq. 21 was satisfied. This means that the necessary and sufficient condition for robustness is satisfied in the range where the intrinsic noise, σ_c, is larger than the extrinsic noise, ΔCa^*.

The range of the fluctuation of PF input satisfying the conditions for robustness is larger in the spine volume than in the cell volume

We next examined the range of the fluctuation of the PF input satisfying the condition for robustness. In the spine

volume in the range considered ($150 \leq Amp_{PF} \leq 215$), Ca^* and P_+ always linearly increase with the increase in Amp_{PF}. Thus, the range of Amp_{PF} where the distribution of Ca_{res} remains the same regardless of CV_a in the spine volume was determined by the range satisfying $\Delta Ca^* \ll \sigma_c$. In the spine volume, $\Delta Ca^*/\sigma_c \ll 1$ when x was small and $\Delta Ca^*/\sigma_c$ increased with the increase in x, and exceeded 1 at $x = 110$ (Fig. 4 *A*). In contrast, in the cell volume, $\Delta Ca^*/\sigma_c$ exceeded 1 even at $x = 2$ (Fig. 4 *B*). We defined δ_{max} as x that gives $\Delta Ca^*/\sigma_c = 1$. δ_{max} relatively provides the upper bound of x where $\Delta Ca^*/\sigma_c \ll 1$. Thus, we used δ_{max} as the index of the range of x for robustness (Fig. 4 *C*). The larger δ_{max} means more robustness. δ_{max} was highest at the spine volume and decreased with the increase in volume (Fig. 4 *C*), indicating that the spine volume gives the highest robustness. Because δ_{max} in the spine volume was much larger than that in the cell volume, the upper bound of x where $\Delta Ca^*/\sigma_c \ll 1$ in the spine volume is much larger than that in the cell volume. Here, x denoted the relative amplitude of the PF input as the displacement of Amp_{PF} from μ_a, the average of Amp_{PF}, given by $x = Amp'_{PF} = Amp_{PF} - \mu_a$, i.e., a larger x corresponds to a larger CV_a. Therefore, in the spine volume, in the range $150 < Amp_{PF} \leq 215$, because $\Delta Ca^*/\sigma_c$ was smaller than 1 even with a larger x, information transfer by Ca_{res} is robust with a larger CV_a. In contrast, in the cell volume, because $\Delta Ca^*/\sigma_c$ was larger than 1 even with a small x, information transfer by Ca_{res} is not robust, even with a small CV_a.

Next, we confirmed that, when $\Delta Ca^*/\sigma_c$ is smaller than 1, the distribution of Ca_{res} with $Amp_{PF} = \mu_a$ and the averaged distribution of Ca_{res} for $Amp_{PF} = \mu_a \pm x$ becomes the same. We quantified the similarities between the two distributions of Ca_{res} by the χ^2 distance. In the spine volume (Fig. 4 *D*, *red*), most of the $\Delta Ca^*/\sigma_c$ were smaller than 1, and the χ^2 distance were also small, indicating that $\Delta Ca^*/\sigma_c$ is smaller than 1 and the two distributions of Ca_{res} are quite similar in the spine volume. In contrast, in the cell volume (Fig. 4 *D*, *blue*), most of the $\Delta Ca^*/\sigma_c$ were larger than 1 and the χ^2 distance were almost 1, indicating that $\Delta Ca^*/\sigma_c$ is larger than 1, and the two distributions of Ca_{res} are quite different. Therefore, when ΔCa^*, the gap of two distributions of Ca_{res}, is smaller than σ_c, the SD of the distribution of Ca_{res}, then the distribution of Ca_{res} does not change and becomes robust against fluctuation of the PF input.

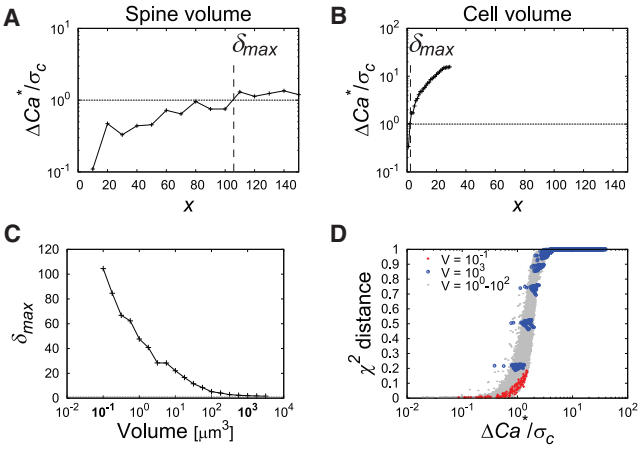

FIGURE 4 The ratio between extrinsic and intrinsic noise, $\Delta Ca^*/\sigma_c$, determines the range of robustness. (*A* and *B*) the relative amplitude of the PF input, x, dependency of $\Delta Ca^*/\sigma_c$ with $\mu_a = 180$ in the spine volume (*A*) and in the cell volume (*B*) are provided. The robustness index δ_{max} is defined as x giving $\Delta Ca^*/\sigma_c = 1$. (*C*) The volume-dependency of δ_{max} for $\mu_a = 180$ is provided. (*D*) The relationship between $\Delta Ca^*/\sigma_c$ and the χ^2 distance between the averaged distribution of the distributions of Ca_{res} with $Amp_{PF} = \mu_a \pm x$ and the distribution of Ca_{res} with $Amp_{PF} = \mu_a$ are provided. The red points, blue points, and gray dots indicate the value obtained in the spine volume, the cell volume, and the intermediate volumes, respectively. To see this figure in color, go online.

In summary, in the spine volume, σ_c, the SD of the distribution of Ca_{res}, is larger than ΔCa^*, the gap of the mode of the distribution of Ca_{res}, which reflects the fluctuation of Amp_{PF}, indicating that the range of x satisfying $\Delta Ca^* \ll \sigma_c$ is wider. This means that the distribution of Ca_{res} with fluctuation of amplitude of the PF input conforms to that without fluctuation of amplitude of the PF input. Moreover, $\Delta Ca^* \ll \sigma_c$ indicates that the distribution of Ca_{res} caused by extrinsic noise, ΔCa^*, is much smaller than that caused by intrinsic noise, σ_c. Hence, the information transfer by Ca_{res} becomes robust against the fluctuation of the amplitude of the PF input. In contrast, in the cell volume, the SD of the distribution of Ca_{res} without fluctuation of the amplitude of the PF input is small, and the averaged distribution of Ca_{res} with fluctuation of the amplitude of the PF input does not conform to that without fluctuation of the amplitude of the PF input. Moreover, $\Delta Ca^* > \sigma_c$ indicates that the distribution gap of Ca_{res} caused by extrinsic noise, ΔCa^*, is larger than that caused by intrinsic noise, σ_c. Hence, the information transfer by Ca_{res} is not robust against fluctuation of amplitude of the PF input.

The mechanism of sensitivity

In the detailed stochastic model, the Ca^{2+} response was more sensitive to lower numbers of PF inputs in the spine volume than the cell volume (23). We tried to examine the sensitivity in the simple stochastic model and defined the "sensitivity" as follows. For each volume, the PF input was given by the Gaussian distribution with the fixed SD, and the average amplitude of the PF input was varied (see Materials and Methods). Amp^* was defined as an index of sensitivity for each volume, with the average amplitude, μ_s, giving the maximum of mutual information. Smaller Amp^* indicates higher sensitivity to the lower amplitude of the PF input.

In the spine volume, the mutual information exhibited the bell-shaped response, where $Amp^* = 100$ gives the maximum mutual information (Fig. 5 *A*, *black line and the white triangle*; Fig. 5 *B*; see Fig. S6, *A* and *F*). With the increase in volume, Amp^* shifted to ~220 (Fig. 5 *A*,

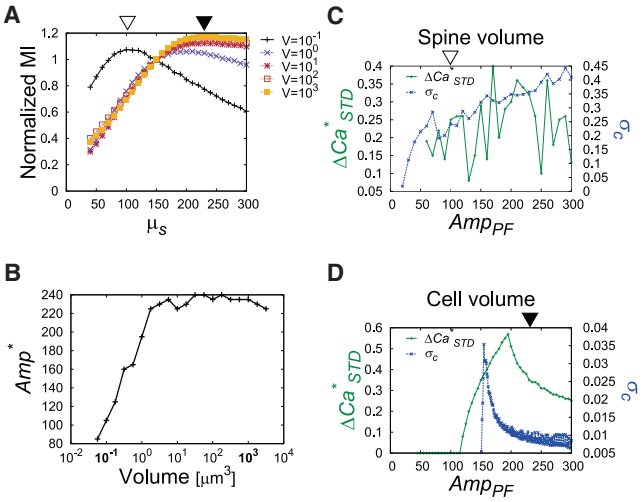

FIGURE 5 The mechanism of sensitivity. (*A*) μ_s, the average of the input distribution of Amp_{PF}, dependency of the mutual information is provided. The mutual information is normalized by the value of that with $\mu_s = 150$. The brighter color indicates the larger volume. The white and black triangles denote Amp^*, the amplitude of the PF input realizing the maximum of the mutual information, in the spine volume and in the cell volume, respectively. $Amp^* = 100$ in the spine volume and $Amp^* = 235$ in the cell volume. The input distribution of Amp_{PF} is utilized as the Gaussian distribution with $STD = 40$, SD. (*B*) The volume-dependency of the amplitude of the PF input realizing the maximum of the mutual information, Amp^* is provided. (*C* and *D*) The Amp_{PF} dependencies of ΔCa^*_{STD}, the dynamic range of the distribution of Ca_{res} for $Ca_{res} > \theta$ (*green*), and σ_c, the SD of the distribution of Ca_{res} (*blue*). $STD = 40$ was used. The white and black triangles denote Amp^* in the spine volume and in the cell volume, respectively. To see this figure in color, go online.

orange line and black triangle; Fig. 5 *B*; see Fig. S6, *E* and *J*). This result indicates that the spine volume shows higher sensitivity to the lower amplitude of the PF input than the larger volume including the cell volume.

We considered the mechanism that the spine shows higher sensitivity to the lower amplitude of the PF input. When the SD of the PF input distribution is the same, the mutual information depends on ΔCa^*_{STD}, the dynamic range of the output, and σ_c, the SD of the output (Fig. S7). For example, when the dynamic range of the output is the same, the smaller SD of the output gives more mutual information. When the SD of the output is the same, the broader dynamic range gives more mutual information. For simplicity, the window width of the input distribution of Amp_{PF} was set as the finite range defined as the average $\pm$ SD of the input distribution of Amp_{PF}, i.e., $\mu_s \pm STD$, and the dynamic range was denoted as the gap of mode of the distribution of Ca_{res} between the upper bound ($Amp_{PF} = \mu_s + STD$) and lower bound ($Amp_{PF} = \mu_s - STD$) of the input distribution of Amp_{PF}, i.e., $\Delta Ca^*_{STD} = Ca^*(\mu_s + STD) - Ca^*(\mu_s - STD)$.

First, we considered ΔCa^*_{STD}, the dynamic range of the output. We defined $\psi(V)$ for each volume of Amp_{PF} as the smallest amplitude of the PF input where the Ca_{res} of some trials exceed θ (see Fig. S8 *A*). In the spine volume, Ca^* linearly increased along Amp_{PF} for $Amp_{PF} > \psi(V)$ (Figs. S5 *C* and S8 *A*); hence, ΔCa^*_{STD} was largely variable and independent of Amp_{PF} (Fig. 5 *C*; see Fig. S8, *B* and *E–H*). In contrast, in the cell volume, ΔCa^*_{STD} was bell-shaped curve with the maximum at $Amp_{PF} = 200$ (Fig. 5 *D*; see Fig. S8, *C* and *U–X*).

Next, we considered σ_c, the SD of Ca_{res} for $Ca_{res} > \theta$. In the spine volume, σ_c gradually increased with the increase in Amp_{PF} for $Amp_{PF} > \psi(10^{-1}) \simeq 50$ (Fig. 5 *C*, *blue line*). In contrast, in the cell volume, σ_c became largest at $Amp_{PF} = \sim 150$ and gradually decreased with the increase in Amp_{PF} (Fig. 5 *D*, *blue line*).

In the spine volume, ΔCa^*_{STD} was almost constant for $Amp_{PF} > 60$ and σ_c increased along Amp_{PF}; therefore, the mutual information became maximum at approximately $Amp_{PF} = 60$ (see Fig. S8, *E–H*, *black dashed line*; also see Fig. S6, *A* and *F*). In contrast, in the cell volume, the mutual information became maximum at $Amp_{PF} = 235$, which is greater than $Amp_{PF} = 200$, giving the maximum of ΔCa^*_{STD} (Fig. 5, *A* and *D*; see Fig. S8, *U–X*, *black dashed line*; also see Fig. S6, *E* and *J*). This is because, that despite the higher ΔCa^*_{STD}, the σ_c was larger and the loss of information became large. Decreasing σ_c resulted in increase of mutual information.

Thus, the mutual information becomes maximum at $Amp_{PF} = 60$ in the spine volume and at $Amp_{PF} = 250$ in the cell volume, indicating the higher sensitivity to lower amplitude of the PF input in the spine volume.

The mechanism of efficiency

We defined the efficiency as the mutual information per PF input. The average of the PF input was given by $\mu_s \times V$, whose dimension is equal to number of molecules. Efficiency means how much information can be transferred by a unitary PF input. Higher mutual information per PF input indicates higher efficiency. The mutual information monotonically increased with the increase in volume, and the rate of the increase of the mutual information decreased with the increase in volume (Fig. 6 *A*, *black*); therefore, the mutual information per PF input monotonically decreased (Fig. 6 *B*, *black line*), indicating that the mutual information per PF input, i.e., the efficiency, was larger in the spine volume and decreased as the volume increased to the cell volume (Fig. 6 *B*, *black line*).

Next, we examined the mechanism of the volume-dependency of the mutual information. The slope of the mutual information decreased with the increase in volume and became close to a logarithmic increase in the larger volume (Fig. 6 *A*, *black*). Then, we assumed that the volume-dependent increase of the mutual information is approximated with constants, a, b, and c (see Materials and Methods), as given by the following:

$$I(Ca_{res}; \Delta t) \simeq a \log_2(b + c \times V). \quad (27)$$

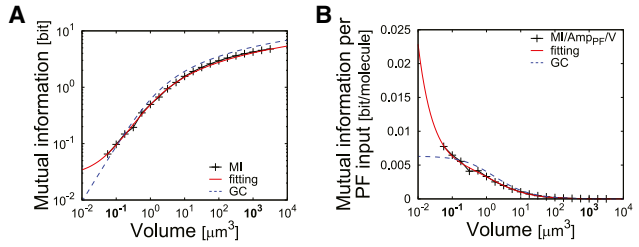

FIGURE 6 The mechanism of efficiency. (*A*) The volume-dependency of the mutual information between Amp_{PF} and Ca_{res} is provided. (*B*) The volume-dependency of the mutual information per PF input, i.e., the efficiency is shown. The total mutual information is shown in black; the fitted curve of the total mutual information with the $a \log_2 (b + c \times V)$ with $a = 0.3924651$, $b = 1.049141$, and $c = 1.330285$, is shown in red; the channel capacity of the Gaussian channel, $1/2 \log_2 (1 + cV)$ with $c = 0.5128671$, is shown in blue (see Materials and Methods). We assume the input distribution of Amp_{PF} as the Gaussian distribution with $\mu_s = 150$, the average of the amplitude of the distribution of the PF input, and $STD = 40$ as the SD of the distribution of the PF input. To see this figure in color, go online.

This function fits well with the volume-dependent mutual information (Fig. 6 *A*, *red line*) and the mutual information per PF input (Fig. 6 *B*, *red line*), indicating that this function captures the features of the volume-dependency of the mutual information in the spine volume and the larger volume.

We also considered the Gaussian channel, which is a simple linear transmission system. For input X, when the system noise Z obeys the Gaussian distribution, the output $Y = X + Z$ also obeys the Gaussian distribution. In this case, under the constraint $E[X^2] < F$, the mutual information (channel capacity) between the input, X, and the output, Y, is simply described as follows:

$$I(Y;X) = \frac{1}{2}\log_2\left(1 + \frac{F}{\sigma_Z^2}\right) \tag{28}$$

where F denotes the power constraint of input and σ_Z denotes the SD of the noise intensity. Here, F is regarded as a constant value because the input distribution for calculating $I(Ca_{res}; \Delta t)$ in Eq. 28 (Fig. 6, *blue line*) is assumed to be unchanged. It has been shown that the SD of reactions is proportional to the power of the number of molecules, i.e., volume, so that the fluctuation of the number of molecules can be approximated as $\sigma_Z'^2 \propto V$ (29). Then, the fluctuation of concentration of the molecules can be approximated by $\sigma_Z^2 = (\sigma_Z'/V)^2 \propto V^{-1}$. Therefore, the mutual information for the Gaussian channel is given by the following:

$$I(Ca_{res}; \Delta t) \simeq \frac{1}{2}\log_2(1 + c \times V) \tag{29}$$

(Fig. 6, *A* and *B*, *blue lines*). Equations 27 and 29 indicate the same volume-dependency of the mutual information. However, in the smaller volume including the spine volume, the mutual information per PF input of the Ca^{2+} response was larger than that of the Gaussian channel (Fig. 6 *B*). This difference in the volume-dependency is likely to be caused by the different values of the parameters, which were $a = 0.3924651$ and $b = 1.049141$ in the fitted function, whereas 1/2 and 1 in the Gaussian channel, respectively. There were other differences in both systems; the noise of the system in this study is not exactly a Gaussian noise, and the input-output relation is nonlinear. Despite such differences, both systems exhibited similar volume-dependency of the mutual information, suggesting that the more efficient information transfer in the smaller volume is a universal property in the general information transduction systems.

DISCUSSION

In this study, we constructed the simple stochastic model of the Ca^{2+} increase in the spine of PF-cerebellar Purkinje cell synapse. The simple stochastic model reproduces consistent properties of information transfer with the detailed stochastic model, indicating that these properties are not lost by the simplification of the model. We clarified the mechanisms of robustness, sensitivity, and efficiency, and we showed that these properties become prominent in the spine volume (Fig. 7). The robustness appears in condition where the SD of the distribution of the Ca^{2+} response, intrinsic noise, is larger than the fluctuation of the distribution of the Ca^{2+} response caused by the PF input fluctuation, extrinsic noise.

Higher sensitivity to a lower amplitude of the PF input requires the wider dynamic range of the Ca^{2+} response and the smaller SD of the distribution of the Ca^{2+} response in the range of the lower amplitude of the PF input. In the spine volume, because of the stochasticity in reactions, even the weak PF input can induce a large Ca^{2+} increase, resulting in a wider dynamic range of the Ca^{2+} response for the lower amplitude of the PF input in the spine volume than in the cell volume. Moreover, the SD of the distribution of the Ca^{2+} response in the range of the lower amplitude of the PF input was small. In the larger volume than the spine volume, the sensitivity abruptly decreased because stronger PF input was required for compensating the large SD of the distribution of the Ca^{2+} response.

The highest efficiency in the spine volume is derived from the nature of the volume-dependency of mutual information; the rate of increase of the mutual information monotonically decreased with the increase in volume. Then, the mutual information per PF input, efficiency, becomes larger in the smaller volume. This result indicates that the spine utilizes the limit of the smallness to acquire the highest efficiency.

Robustness appears when intrinsic noise is larger than extrinsic noise. Sensitivity appears because of the stochasticity in the Ca^{2+} increase. Efficiency appears because of the nature of the volume-dependency of information transfer. These characteristics and the underlying mechanisms emerge from the effect of the small volume of the spine,

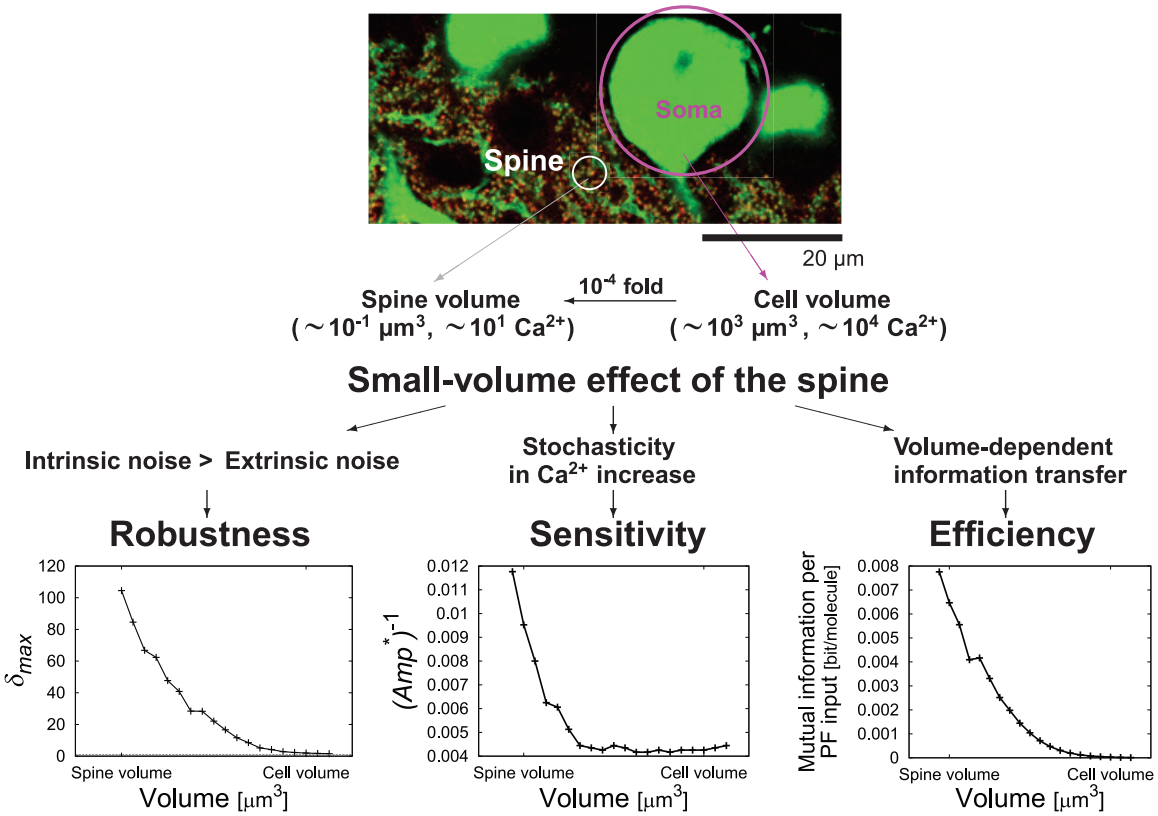

FIGURE 7 Summarizing figure. The small-volume effect enables the spine to have robust, sensitive, and efficient information transfer. Robustness appears when intrinsic noise is larger than extrinsic noise. Sensitivity appears because of the stochasticity in Ca^{2+} increase. Note that, as index for the sensitivity in this figure, the inverse of *Amp** (Fig. 5 *B*) is used. Efficiency appears because of the nature of the volume-dependency of information transfer. To see this figure in color, go online.

which we denote "the small-volume effect." The small-volume effect enables the spine to have robust, sensitive, and efficient information transfer. The small-volume effect may be seen not only in spines but also in other small intracellular organelles; it comprises the general strategy for biological information transfer. The small-volume effect is one of the reasons why the spine has to be so small. The small-volume effect is also equivalent to the effect of small numbers of molecules, with the small-number effect suggesting that the robustness, sensitivity, and efficiency can also be seen under the conditions where numbers of molecules are limited even in a larger volume. Naturally, the reasons why the spine is so small are not only the above-mentioned small-volume effect, but also to obtain the extremely small diffusion space, to increase the surface area in limited volume, to compartmentalize the biochemical reaction field, etc. However, regarding the informatic advantage, the smallness of the spine provides the robust, sensitive, and efficient information transfer.

In addition, the information transfer in the spine volume is much less than 1 bit, indicating that the information transfer in a spine is insufficient to reliably determine even a binary decision. Despite the low reliability of a single spine, summation of the Ca^{2+} response in many spines may overcome the amplitude of the Ca^{2+} in a cell in terms of the reliability of information transfer. Thus, the smallness and numerosity of spines may be a unique strategy to realize robust, sensitive, and efficient information transfer in neurons. Furthermore, the information transfer by numerous spines can be reliable to realize the motor control and cerebellar learning through the long-term depression (LTD) (13,14).

It has been known that in most excitatory synapses, the Ca^{2+} increase in the spine, evoked by glutamate released from the presynaptic fiber, is mainly mediated by N-methyl-D-aspartate receptors (NMDAR), another glutamate-gated ion channel that, in contrast to the receptors of the PF-Purkinje cell synapse, such as AMPA and metabotropic glutamate receptors (mGluR1), are endowed with a high Ca^{2+} permeability (30,31). In the future, we will analyze whether the Ca^{2+} increase mediated by NMDAR in the spine also shows robustness, sensitivity, and efficiency and study whether such properties are receptor-type-specific or are conserved among different varieties of spine regardless of the type of the receptors.

In general, most of artificial devices for information transfer have physical limitations in design. For example, in design of electrical devices, the limitations of space and

power consumption critically determine the upper bound of performance. The strategy for the information transfer in the spine looks to be opposite to those in these devices, however, and the small-volume effect may provide the new design principle of devices for information transfer.

SUPPORTING MATERIAL

Supporting Materials and Methods, eight figures, and two tables are available at http://www.biophysj.org/biophysj/supplemental/S0006-3495(17)30037-1.

AUTHOR CONTRIBUTIONS

M.F. and S.K. conceived the project. M.F. constructed the model and performed the stochastic simulation. M.F., K.O., Y.K., M.H., and S.K. analyzed the data. M.F. and K.O. contributed theoretical analysis. M.F. and S.K. wrote the manuscript.

ACKNOWLEDGMENTS

We are grateful to Dr. Hidetoshi Urakubo, Dr. Takuya Koumura, Dr. Shinsuke Uda, Dr. Yuichi Sakumura and our laboratory members for their critical reading of this manuscript, and Dr. Tamiki Komatsuzaki for fruitful discussion.

This work was supported by The Creation of Fundamental Technologies for Understanding and Control of Biosystem Dynamics, CREST, from the Japan Science and Technology (JST). M.F. was funded by the Japan Society for the Promotion of Science (JSPS) (JSPS Grants-in-Aid for Scientific Research (KAKENHI) grant No. 6K12508).

REFERENCES

1. Napper, R. M., and R. J. Harvey. 1988. Number of parallel fiber synapses on an individual Purkinje cell in the cerebellum of the rat. *J. Comp. Neurol.* 274:168–177.
2. Stuart, G., N. Spruston, and M. Häusser. 2007. Dendrites. Oxford University Press, Oxford, UK.
3. Lee, K. J., H. Kim, and I. J. Rhyu. 2005. The roles of dendritic spine shapes in Purkinje cells. *Cerebellum.* 4:97–104.
4. Harris, K. M., and J. K. Stevens. 1988. Dendritic spines of rat cerebellar Purkinje cells: serial electron microscopy with reference to their biophysical characteristics. *J. Neurosci.* 8:4455–4469.
5. Rapp, M., I. Segev, and Y. Yarom. 1994. Physiology, morphology and detailed passive models of guinea-pig cerebellar Purkinje cells. *J. Physiol.* 474:101–118.
6. Takács, J., and J. Hámori. 1994. Developmental dynamics of Purkinje cells and dendritic spines in rat cerebellar cortex. *J. Neurosci. Res.* 38:515–530.
7. Antunes, G., and E. De Schutter. 2012. A stochastic signaling network mediates the probabilistic induction of cerebellar long-term depression. *J. Neurosci.* 32:9288–9300.
8. Anwar, H., I. Hepburn, …, E. De Schutter. 2013. Stochastic calcium mechanisms cause dendritic calcium spike variability. *J. Neurosci.* 33:15848–15867.
9. Barbour, B. 1993. Synaptic currents evoked in Purkinje cells by stimulating individual granule cells. *Neuron.* 11:759–769.
10. Okubo, Y., H. Sekiya, …, M. Iino. 2010. Imaging extrasynaptic glutamate dynamics in the brain. *Proc. Natl. Acad. Sci. USA.* 107:6526–6531.
11. Isope, P., and B. Barbour. 2002. Properties of unitary granule cell→Purkinje cell synapses in adult rat cerebellar slices. *J. Neurosci.* 22:9668–9678.
12. Ito, M. 1970. Neurophysiological aspects of the cerebellar motor control system. *Int. J. Neurol.* 7:162–176.
13. Kawato, M. 1999. Internal models for motor control and trajectory planning. *Curr. Opin. Neurobiol.* 9:718–727.
14. Kawato, M., S. Kuroda, and N. Schweighofer. 2011. Cerebellar supervised learning revisited: biophysical modeling and degrees-of-freedom control. *Curr. Opin. Neurobiol.* 21:791–800.
15. Miyakawa, H., V. Lev-Ram, …, W. N. Ross. 1992. Calcium transients evoked by climbing fiber and parallel fiber synaptic inputs in guinea pig cerebellar Purkinje neurons. *J. Neurophysiol.* 68:1178–1189.
16. Wang, S. S., W. Denk, and M. Häusser. 2000. Coincidence detection in single dendritic spines mediated by calcium release. *Nat. Neurosci.* 3:1266–1273.
17. Ito, M. 2002. The molecular organization of cerebellar long-term depression. *Nat. Rev. Neurosci.* 3:896–902.
18. Mauk, M. D., K. S. Garcia, …, P. M. Steele. 1998. Does cerebellar LTD mediate motor learning? Toward a resolution without a smoking gun. *Neuron.* 20:359–362.
19. Steinmetz, J. E. 1990. Classical nictitating membrane conditioning in rabbits with varying interstimulus intervals and direct activation of cerebellar mossy fibers as the CS. *Behav. Brain Res.* 38:97–108.
20. Doi, T., S. Kuroda, …, M. Kawato. 2005. Inositol 1,4,5-trisphosphate-dependent Ca2+ threshold dynamics detect spike timing in cerebellar Purkinje cells. *J. Neurosci.* 25:950–961.
21. Honda, M., H. Urakubo, …, S. Kuroda. 2013. A common framework of signal processing in the induction of cerebellar LTD and cortical STDP. *Neural Netw.* 43:114–124.
22. Honda, M., H. Urakubo, …, S. Kuroda. 2011. Analysis of development of direction selectivity in retinotectum by a neural circuit model with spike timing-dependent plasticity. *J. Neurosci.* 31:1516–1527.
23. Koumura, T., H. Urakubo, …, S. Kuroda. 2014. Stochasticity in Ca2+ increase in spines enables robust and sensitive information coding. *PLoS One.* 9:e99040.
24. Cao, Y., D. T. Gillespie, and L. R. Petzold. 2006. Efficient step size selection for the tau-leaping simulation method. *J. Chem. Phys.* 124:044109.
25. Gillespie, D. T., A. Hellander, and L. R. Petzold. 2013. Perspective: stochastic algorithms for chemical kinetics. *J. Chem. Phys.* 138:170901.
26. Cheong, R., A. Rhee, …, A. Levchenko. 2011. Information transduction capacity of noisy biochemical signaling networks. *Science.* 334:354–358.
27. Shannon, C. E. 1948. A mathematical theory of communication. *Bell Syst. Tech. J.* 27:379–423.
28. Rancz, E. A., and M. Häusser. 2006. Dendritic calcium spikes are tunable triggers of cannabinoid release and short-term synaptic plasticity in cerebellar Purkinje neurons. *J. Neurosci.* 26:5428–5437.
29. Wang, J., and P. Wolynes. 1995. Intermittency of single molecule reaction dynamics in fluctuating environments. *Phys. Rev. Lett.* 74:4317–4320.
30. Li, F., and J. Z. Tsien. 2009. Memory and the NMDA receptors. *N. Engl. J. Med.* 361:302–303.
31. Furukawa, H., S. K. Singh, …, E. Gouaux. 2005. Subunit arrangement and function in NMDA receptors. *Nature.* 438:185–192.